



HAL
open science

Single Breath-Hold MR Elastography for Fast Biomechanical Probing of Pancreatic Stiffness

Anne-sophie van Schelt, Lukas Gottwald, Nienke P.M. Wassenaar, Jurgen Runge, Ralph Sinkus, Jaap Stoker, Aart Nederveen, Eric Schrauben

► **To cite this version:**

Anne-sophie van Schelt, Lukas Gottwald, Nienke P.M. Wassenaar, Jurgen Runge, Ralph Sinkus, et al.. Single Breath-Hold MR Elastography for Fast Biomechanical Probing of Pancreatic Stiffness. *Journal of Magnetic Resonance Imaging*, 2023, 10.1002/jmri.28773 . hal-04302479

HAL Id: hal-04302479



<https://hal.science/hal-04302479v1>




Submitted on 23 Nov 2023

HAL is a multi-disciplinary open access archive for the deposit and dissemination of scientific research documents, whether they are published or not. The documents may come from teaching and research institutions in France or abroad, or from public or private research centers.

L'archive ouverte pluridisciplinaire **HAL**, est destinée au dépôt et à la diffusion de documents scientifiques de niveau recherche, publiés ou non, émanant des établissements d'enseignement et de recherche français ou étrangers, des laboratoires publics ou privés.

Single Breath-Hold MR Elastography for Fast Biomechanical Probing of Pancreatic Stiffness

Anne-Sophie van Schelt, MSc,^{1,2*}  Lukas M. Gottwald, PhD,¹ 

Nienke P.M. Wassenaar, MSc,^{1,2}  Jurgen H. Runge, MD, PhD,^{1,3}  Ralph Sinkus, PhD,^{4,5} 

Jaap Stoker, MD, PhD,^{1,6}  Aart J. Nederveen, PhD,¹  and Eric M. Schrauben, PhD¹ 

Background: Pancreatic ductal adenocarcinoma (PDAC) stromal disposition is thought to influence chemotherapy efficacy and increase tissue stiffness, which could be quantified noninvasively via MR elastography (MRE). Current methods cause position-based errors in pancreas location over time, hampering accuracy. It would be beneficial to have a single breath-hold acquisition.

Purpose: To develop and test a single breath-hold three-dimensional MRE technique utilizing prospective undersampling and a compressed sensing reconstruction (CS-MRE).

Study Type: Prospective.

Population: A total of 30 healthy volunteers (HV) (31 ± 9 years; 33% male) and five patients with PDAC (69 ± 5 years; 80% male).

Field Strength/Sequence: 3-T, GRE Ristretto MRE.

Assessment: First, optimization of multi breath-hold MRE was done in 10 HV using four combinations of vibration frequency, number of measured wave-phase offsets, and TE and looking at MRE quality measures in the pancreas head. Second, viscoelastic parameters delineated in the pancreas head or tumor of CS-MRE were compared against (I) 2D and (II) 3D four breath-hold acquisitions in HV ($N = 20$) and PDAC patients. Intrasession repeatability was assessed for CS-MRE in a subgroup of healthy volunteers ($N = 15$).

Statistical Tests: Tests include repeated measures analysis of variance (ANOVA), Bland–Altman analysis, and coefficients of variation (CoVs). A P -value $< .05$ was considered statistically significant.

Results: Optimization of the four breath-hold acquisitions resulted in 40 Hz vibration frequency, five wave-phases, and echo time (TE) = 6.9 msec as the preferred method (4BH-MRE). CS-MRE quantitative results did not differ from 4BH-MRE. Shear wave speed (SWS) and phase angle differed significantly between HV and PDAC patients using 4BH-MRE or CS-MRE. The limits of agreement for SWS were $[-0.09, 0.10]$ m/second and the within-subject CoV was 4.8% for CS-MRE.

Data Conclusion: CS-MRE might allow a single breath-hold MRE acquisition with comparable SWS and phase angle as 4BH-MRE, and it may still enable to differentiate between HV and PDAC.

Level of Evidence: 2

Technical Efficacy Stage: 2

J. MAGN. RESON. IMAGING 2023.

Pancreatic ductal adenocarcinoma (PDAC) is the fourth leading cause of cancer-related deaths worldwide, with a 5-year survival of 8%.¹ Treatment with systemic chemotherapy

increases overall survival and can render previously irresectable patients eligible for resection.² However, chemotherapy has a poor performance status with a treatment efficacy of only

View this article online at wileyonlinelibrary.com. DOI: 10.1002/jmri.28773

Received Mar 6, 2023, Accepted for publication Apr 26, 2023.

*Address reprint requests to: A.-S. van Schelt, Meibergdreef 9, Z0-178, 1105 AZ Amsterdam, The Netherlands. E-mail: a.vanschelt@amsterdamumc.nl

From the ¹Department of Radiology and Nuclear Medicine, Amsterdam UMC, University of Amsterdam, Amsterdam, The Netherlands; ²Imaging and Biomarkers, Cancer Center Amsterdam, Amsterdam, The Netherlands; ³Department of Radiology, Netherlands Cancer Institute, Amsterdam, The Netherlands;

⁴Imaging Sciences and Biomedical Engineering, Kings College London, London, UK; ⁵Department of Radiology, Université de Paris, Paris, France; and

⁶Endocrinology, Amsterdam Gastroenterology, Amsterdam, The Netherlands

This is an open access article under the terms of the [Creative Commons Attribution-NonCommercial-NoDerivs](https://creativecommons.org/licenses/by-nc-nd/4.0/) License, which permits use and distribution in any medium, provided the original work is properly cited, the use is non-commercial and no modifications or adaptations are made.

36% (for becoming eligible for surgery) and has a high toxicity, reducing quality of life.³

Typically, PDAC is characterized by prolific stromal deposition, and recently it has been hypothesized that this stromal deposition affects chemotherapy efficacy.⁴ As stromal deposition, tumor, and surrounding healthy tissue may all have differing biomechanical properties, the local tissue stiffness could be a potential biomarker to predict stromal deposition and hence chemotherapy efficacy,⁵ which has been exploited in, for example, diffusion MRI.⁶ As such, prior insight in the underlying mechanical structure of a pancreatic tumor could influence treatment plans.

Imaging by MR elastography (MRE) allows for non-invasive determination of tissue visco-elastic properties.⁷ Longitudinal (over time) or local (over space) differences in tissue stiffness might add to the growing knowledge of pancreatic disease pathophysiology. Specifically, MRE research to date has mainly focused on large organs, such as the liver and brain.⁸ Assessment of the pancreas with MRE remains challenging due to its small size, elongated shape, and central abdominal location. Shear wave quality is paramount to obtaining reliable results regarding biomechanics, which rely on the analysis and reconstruction of the propagation of shear waves into and through the pancreas.⁷ Consequently, pancreatic MRE requires careful MRI sequence parameter optimization. Moreover, the quantitative accuracy of MRE in small structures depends on the local stability of the tissue being imaged over all wave-offsets and motion-encoding directions.⁹ Multiple abdominal MRE acquisition strategies have been reported, which include three-dimensional (3D) MRE using spin-echo echo planar imaging (SE-EPI) in six breath-holds,¹⁰ multi-slice multi-frequency SE-EPI in free-breathing,^{11,12} gradient-echo (GRE) EPI in three consecutive breath-holds,¹³ and GRE sequences in breath-holding.¹⁴ Free-breathing acquisitions are more comfortable for patients, however they introduce respiratory-dependent position-based errors in spatial sampling of consecutive wave-phase (WP) offsets throughout the acquisition, when sequence repetition time (TR) and respiratory rhythm are not in sync.

The reference MRE acquisition method at our institution is the Ristretto sequence in combination with a gravitational transducer.^{15,16} The Ristretto sequence is a generalized multi-shot GRE acquisition with fractional motion encoding, encompassing an intrinsic delay for optimal acquisition.¹⁵ The gravitational transducer relies on the centrifugal force exerted on the transducer casing by an eccentric rotational mass. This method requires four consecutive (~16 seconds) breath-holds, which may introduce respiratory position-based errors in pancreas location, limit spatial and temporal resolution, and can be particularly uncomfortable for patients.^{17,18}

Compressed sensing (CS) is an acceleration technique that uses prospective incoherent undersampling of k-space paired with an iterative reconstruction algorithm using a

Table 1. Scan Parameters for the Three Experiments: Pancreatic MRE Optimization, Compressed Sensing, and Repeatability

	1. Pancreatic MRE optimization combinations				2. Compressed Sensing			3. Repeatability	
	A	B	C	D	(I)	(II)	(III)	CS1	CS2
Acquisition	MS	MS	MS	MS	MS	3D	3D	3D	3D
Acceleration	Sense2	Sense2	Sense2	Sense2	Sense2	Sense2.7	CS 12	CS 12	CS 12
BH time (seconds)	4 × 16	4 × 16	4 × 18	4 × 21	4 × 18	4 × 20	1 × 18	1 × 18	1 × 18
TR/TE (msec)	10/6.9	10/6.9	10/6.9	12/9.2	10/6.9	15/6.9	15/6.9	15/6.9	15/6.9
Flip angle (°)	20	20	20	20	20	10	10	10	10
MEG frequency (Hz)	184	184	184	129	184	179	179	179	179
No. of wave-phase offsets	4	4	5	4	5	5	5	5	5
Vibration frequency (Hz)	50	40	40	40	40	40	40	40	40

In experiment 2, the TR and flip angle were adjusted to accommodate for the 3D acquisition.

MS, multi-slice; 3D, three-dimensional; CS, compressed sensing, with acceleration factor 12; BH, breath-hold; TR, effective repetition time defined as one image-shot; TE, echo time; MEG, motion encoding gradient. Sense = sensitivity encoding acceleration in the phase encoding direction with an acceleration factor 2 or 2.7.

sparsifying transformation and nonlinear optimization.¹⁹ This allows for faster image acquisition while maintaining similar image quality, and to date CS has been used in a number of MRI techniques in multiple organs of the body.^{20–22} While not previously investigated, this suggests that CS could be used to accelerate the MRE acquisition to a single breath-hold, whilst still providing reliable and high-quality images.

The aim of this study was twofold: 1) to optimize the rapid interleaved (Ristretto) GRE acquisition for pancreatic MRE, and 2) to develop and test a prospectively under-sampled and CS-reconstructed single breath-hold 3D MRE in the pancreas.

Materials and Methods

This prospective study was approved by the local institutional review board and all participants gave written informed consent. A total number of 30 healthy volunteers and five patients diagnosed with PDAC were included. Patients were recruited in the context of a larger project on the assessment of pancreatic stiffness using MRE. Patients were eligible with pathological proven PDAC independent of staging or prior treatment and were >18 years old. Healthy volunteers were excluded when they had a history concerning pancreatic diseases (such as pancreatitis, pancreatic masses, or diabetes mellitus) and were under the age of 18.

All scanning was done at 3.0 T (Ingenia, Philips, Best, the Netherlands) with participants positioned head first supine. All participants fasted hours prior to scanning. A gravitational transducer was used, which uses an eccentric mass to induce shear waves in the abdomen.¹⁶ The transducer with a 3D-printed curved polyactic-plate (to increase the contact area of the transducer with the participant) was strapped at the approximate level of the pancreas head. A reusable gel pad was placed between the transducer plate and the participant for more comfort and better wave transmission. The axial field of view (FOV) was: 336 × 192 × 27 mm and 384 × 252 × 27 mm depending on participant size, with (3 mm³) isotropic voxels in nine slices. T2-weighted images were acquired for anatomical reference for every participant (voxel size 1.2 × 1.2 × 3 mm, 20 slices, TR/echo time [TE] = 378/80 msec).

The aims are accomplished in three consecutive experiments: 1) the application of Ristretto GRE-MRE (hereafter, MS-MRE) in the pancreas is optimized in healthy volunteers; 2) the feasibility of pancreatic CS-MRE is assessed and optimized in healthy volunteers and PDAC patients; and 3) the repeatability of CS-MRE is assessed in healthy volunteers.

Experiment 1: Optimization of Multi Breath-Hold Ristretto GRE-MRE for Pancreas

In this experiment we describe the optimization of fractionally encoded multi breath-hold multi-slice GRE-MRE in the pancreas. This was performed in 10 healthy volunteers (female = 4, mean

Table 2. Baseline characteristics of the healthy volunteer cohorts and patient cohort

Characteristics	Healthy Volunteers	PDAC Patients				
		1	2	3	4	5
Age (years)	30.9 ± 9.2	68	63	73	76	67
Sex (% male)	33%	M	M	M	M	F
Weight (kg)	70.8 ± 9.3	70	90	82	81	62
Height (cm)	176 ± 8	170	178	190	185	169
BMI (kg/m ²)	22.9 ± 2	24	28	23	24	22
Diagnosis at time of MRI	-	2	2	1	3	3
Resectable PDAC (1)						
Metastatic PDAC (2)						
LAPC (3)						
Tumor location	-	1	3	2	2	1
Head (1)						
Corpus (2)						
Tail (3)						
Chemotherapy (sessions)	-	>12	>8	0	0	>12
Time after diagnosis (months)	-	8	11	1	1	2
Average tumor size (mm)	-	20	6	7	3	4

BMI, body mass index; PDAC, pancreatic ductal adenocarcinoma; MRI, magnetic resonance imaging, M, male, F, female.

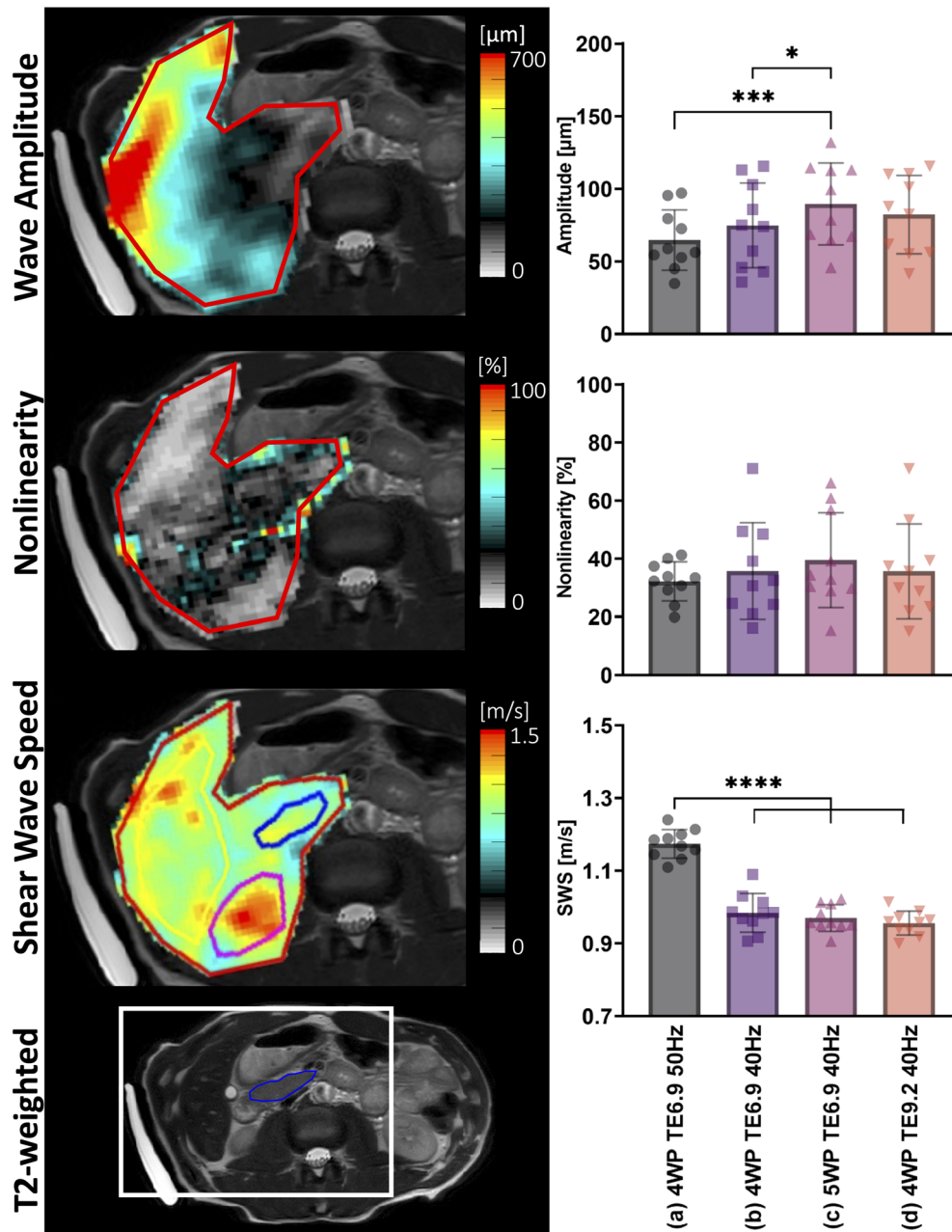


FIGURE 1: (Left) T2-weighted image of a representative volunteer with the pancreas delineated in blue on bottom. The subsequent images for the optimal method of the wave amplitude, nonlinearity, and shear wave speed map delineated in red from top to bottom. On the shear wave speed map the pancreas, liver, and kidney are delineated in blue, yellow, and purple, respectively. (Right) From top to bottom: the average wave amplitude, the average nonlinearity, and the average shear wave speed (SWS) in the pancreas head for each method (* $P = .01$, *** $P \leq .001$, **** $P \leq .0001$).

age = 27 ± 3 years) using four combinations of vibration frequency, number of measured WP offsets, and TE. Table 1 provides a summary of the different combinations tested and motivations for the optimization parameters are given below.

Consideration for the lower vibration frequency was based on a deeper penetration depth, which potentially is beneficial for application in the pancreas.²³ This is a trade-off between penetration depth and longer wavelengths for lower frequencies, which decreases resolution of elastographic details. Furthermore, a higher number of WP offsets can improve accuracy of the reconstruction

algorithm, as it increases number of sampling points. Lastly, a longer TE allows for longer motion-encoding gradients, which increases the phase accrual caused by the wave-induced displacement of tissue. This improves the accuracy of shear wave quantification in regions of low wave amplitude due to an increased sensitivity to motion. However, it prolongs breath-hold duration, which should be below a clinically feasible breath-hold time (15–20 seconds²⁴).

The preferred acquisition strategy was established by determining which acquisition showed the parameters with the highest

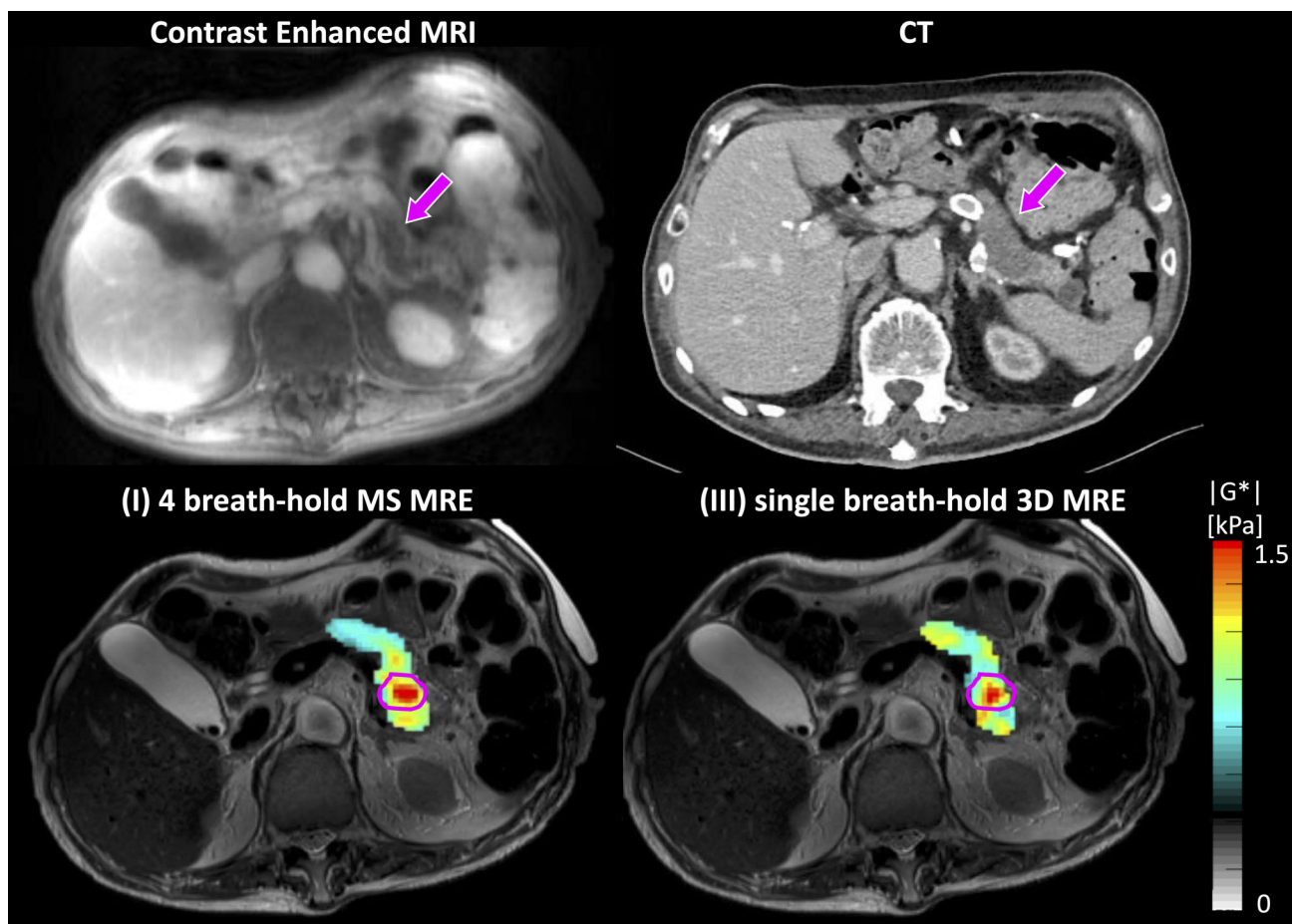


FIGURE 2: Shear wave speed maps of the pancreas overlaid on T2-weighted images of a 73-year-old male patient with pancreatic ductal adenocarcinoma from left to right: scan I (MS 4BH) and scan III (CS-MRE) with the tumor delineated in purple.

quality for the pancreas. The highest quality was defined as the method with the highest MRE quality parameters, which are described in postprocessing.

Experiment 2: Implementation of Prospective Undersampling and CS Reconstruction for Single Breath-Hold Ristretto GRE-MRE

Single breath-hold 3D Ristretto GRE-MRE testing was performed on 20 healthy volunteers (female = 11, mean age = 30 ± 8 years). In addition, five PDAC patients were included (male = 4, mean age = 69 ± 5 years). MRE acquisitions were performed using the determined optimized parameters from experiment 1: nine slices with 40 Hz vibration frequency, 5 WP, and TE = 6.9 msec. Three consecutive pancreatic MRE scans were performed: (I) standard multi-slice (MS) in four breath-holds (MS-MRE); (II) 3D four breath-hold acquisition (3D-MRE); and (III) 3D CS-accelerated single breath-hold acquisition (CS-MRE). Scan parameters are reported in Table 1. In patients, placement of the gravitational transducer was guided by the T2-weighted images to be as close as possible to the tumor. Patients underwent scans I and III only, to limit scan time and number of breath-holds.

To incorporate prospective CS undersampling a 3D acquisition is recommended, as it gives more freedom in optimal undersampling pattern design.²⁵ Incoherent undersampling was

achieved using a variable-density Poisson disc, which was varying in undersampling patterns in the WP offset dimension, repeated for each encoding direction.²⁶ Furthermore, a phase-conjugate symmetry method (half-scan) in both k_y (67%) and k_z (89%) directions was introduced. Acceleration factors were chosen to ensure a clinically feasible breath-hold duration (<18 seconds). For CS acquisitions, reconstruction was performed offline using ReconFrame (version 4.4.4, Gyrotools, Zurich, Switzerland) in MATLAB (version 2021a; The MathWorks Inc., Natick, MA, USA) together with the Berkeley Advanced Reconstruction Toolbox (version 0.5.00, BART; <https://mricon.github.io/bart/>) using a total variation sparsifying transform in time ($\lambda = 0.01$, 50 iterations).²⁷ The sparsifying transform was applied in the WP offset dimension.

Experiment 3: Repeatability of Compressed Sensing

Repeatability of in vivo CS-MRE was tested in 15 of the 20 healthy volunteers who had undergone experiment 2 (female = 10, mean age = 32 ± 8 years). Two consecutive single breath-hold MRE acquisitions were performed without repositioning, to test the within-session repeatability. Prospective CS undersampling and reconstruction were done in the same manner as described earlier.

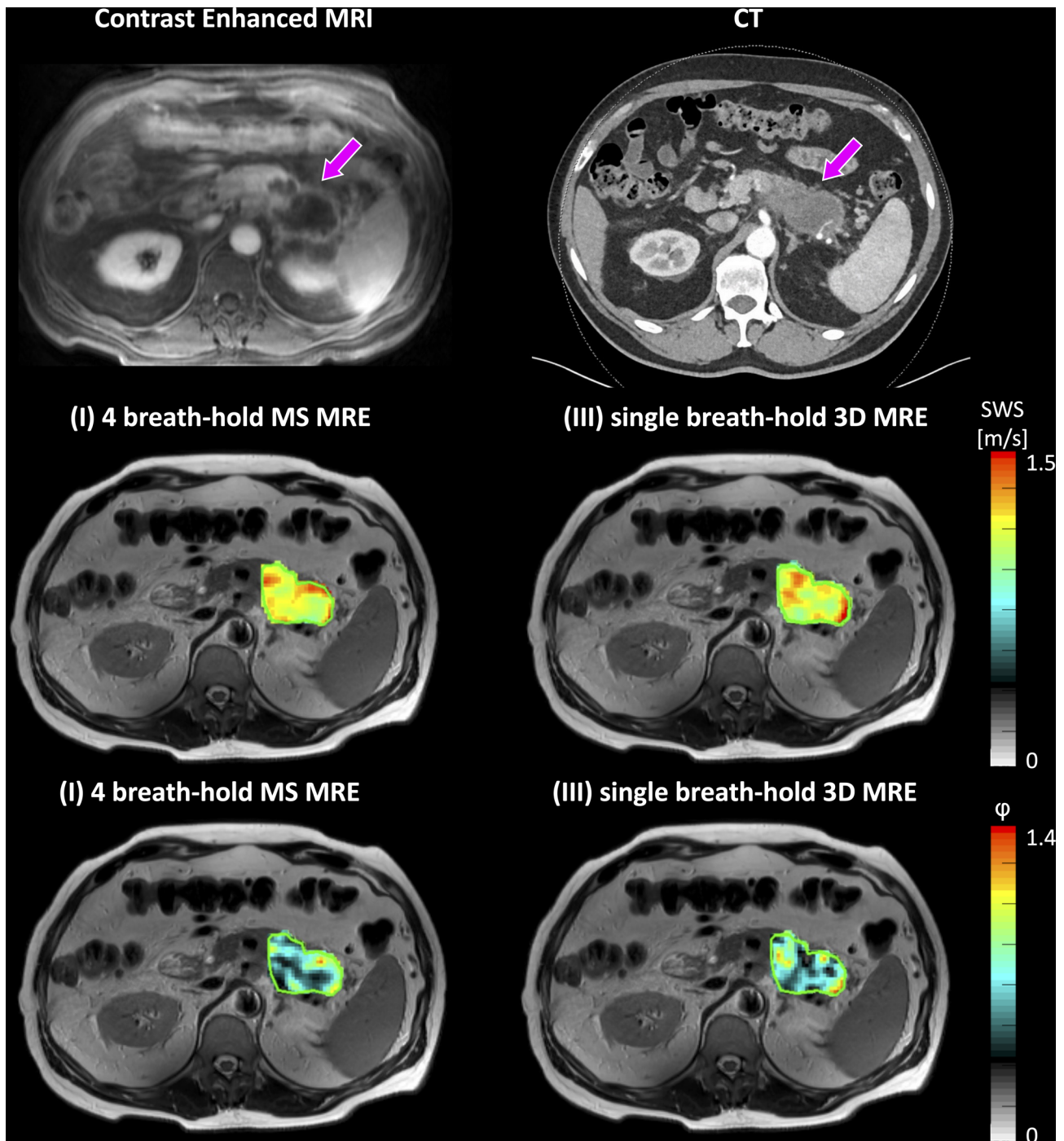


FIGURE 3: Shear wave speed and phase angle maps of the pancreas overlaid on T2-weighted images of a 63-year-old male patient with pancreatic ductal adenocarcinoma from left to right: scan I (MS 4BH) and scan III (CS-MRE) with the tumor delineated in purple.

Postprocessing

Inversion of the data to extract the visco-elastic properties was done using dedicated software (ROOT, as described by Fovargue et al).²⁸ Briefly, phase data were unwrapped and smoothed, and a Gaussian filter was applied ($\sigma = 0.75$, $3 \times 3 \times 3$ pixels) before a 3D Fourier transformation was applied using a 3D Blackman-Harris window. This resulted in a 3D shear wave field. The shear wave displacement was calculated locally per voxel and a finite element method was used to extract the visco-elastic properties, including shear wave

speed (SWS), phase angle (ϕ), elasticity (G_d), and viscosity (G_v). Visco-elastic properties were depicted spatially in an elastogram. Average visco-elastic values were calculated by manually drawing regions of interest (ROIs) on the anatomical magnitude elastography images over the pancreatic head and the tumor for healthy volunteers and patients, respectively. ROIs were drawn by a researcher (AS) with over 4 years of experience in pancreatic MRI. Parameters that were used to compare data quality were the local shear wave amplitude, the nonlinearity, and wave signal-to-noise ratio (SNR).

The nonlinearity gives an indication of the deviation of the phase signal from a perfect sinusoidal wave and should be below 50%.²⁹ The process of drawing ROIs was done with careful consideration of the nonlinearity. The $|q|/|div|$, or wave SNR, is the curl of the displacement vector field over the divergence of the vector field (which is zero up to 10^{-6} precision due to the incompressible nature of tissue), with a higher ratio indicating increased quality.

Statistical Analysis

Statistical testing was done using SPSS (version 28; IBM Corp., Armonk, NY, USA). Repeatability was assessed using Bland–Altman analysis³⁰ and between-subject and within-subject coefficients of variation (CoVs). Data were tested for normality using the Shapiro–Wilk test. Comparison between healthy volunteers and patients was done using an unpaired t test or Mann–Whitney U test in case of skewed data separately for scans I and III to verify if differences in visco-elastic parameters remain after acceleration. Repeated measures of analysis of variance (ANOVA) were performed with a subsequent multiple comparisons with a Bonferroni correction. Data are expressed as mean \pm standard deviation (SD) or median (ranges) as appropriate. An (adjusted) P -value $<.05$ was considered statistically significant.

Results

Study Population

The clinical population consisted of five patients diagnosed with PDAC, regardless of staging, supplemented by 30 healthy volunteers. Three patients received chemotherapy treatment before scanning. One of the five patients underwent a resection 1 week after inclusion. Baseline characteristics are presented in Table 2.

Experiment 1: Optimization of Multi Breath-Hold Ristretto GRE-MRE for Pancreas

Results of experiment 1 are shown in Fig. 1. The mean shear wave amplitude in the pancreas head was observed to be 65 ± 21 , 75 ± 29 , 90 ± 28 , and 82 ± 27 μm for combinations A, B, C, and D, respectively. Statistical analysis exhibited significant differences between the four methods ($F[3, 27] = 11$). Combination C displayed a significant increase in shear wave amplitude when compared to combination A and B. While A–B ($P = .560$), A–D ($P = .076$), B–D ($P = .118$), and C–D ($P = 1.000$) remained constant. Nonlinearity showed no significant differences between all combinations ($F[3, 27] = 1.5$, $P = .232$). The average shear wave speed was 1.17 ± 0.23 , 0.97 ± 0.2 , 0.98 ± 0.2 , and 0.96 ± 0.19 m/second for combinations A, B, C, and D, respectively. Multiple comparisons demonstrated a significant difference in SWS between combination A–B, A–C, and A–D.

The preferred approach was identified as combination C (40 Hz vibration frequency, 5 WP offsets, and a TE of 6.9 msec) due to the significantly higher shear wave amplitude, absence of variations in shear wave speed and

Table 3. Mean \pm SD or Median (IQR) Values for Healthy Volunteers for Different Quality and Visco-Elastic Parameters of MRE and Mean Values for Visco-Elastic Parameters of PDAC Patients

	MRE Quality Parameters			Visco-Elastic Parameters			
	Nonlinearity (%)	Wave SNR	STDEV SWS (m/second)	SWS (m/second)	ϕ (-)	G_d (kPa)	G_l (kPa)
Healthy volunteers (N = 20)							
(I) MS 4BH	44 \pm 8	2.2 \pm 0.8	0.09 \pm 0.04	0.97 \pm 0.07	0.25 \pm 0.13	0.73 \pm 0.08	0.32 \pm 0.19
(II) 3D 4BH	38 \pm 12	3.7 \pm 1.9	0.10 \pm 0.04	0.99 \pm 0.07	0.27 (0.22)	0.77 \pm 0.10	0.40 (0.28)
(III) CS 1BH	47 \pm 17	3.4 \pm 2.7	0.13 \pm 0.09	1.00 (0.14)	0.27 (0.20)	0.80 \pm 0.12	0.40 (0.31)
PDAC patients (N = 5)							
(I) MS 4BH	57 \pm 13	1.7 \pm 0.3	0.17 \pm 0.09	1.19 (0.28)	0.43 (0.24)	1.05 (0.28)	0.77 \pm 0.43
(III) CS 1BH	52 \pm 11	1.6 \pm 0.3	0.16 \pm 0.08	1.29 \pm 0.19	0.44 \pm 0.11	1.17 \pm 0.31	0.62 \pm 0.43

SWS, shear wave speed; ϕ , phase angle; G_d , elasticity; G_l , viscosity; MRE, magnetic resonance elastography; SNR, signal-to-noise ratio; STDEV, standard deviation, SWS, shear wave speed; MS 4BH, multi-slice four breath-hold; 3D 4BH, three-dimensional four breath-hold, CS 1BH, compressed sensing single breath-hold.

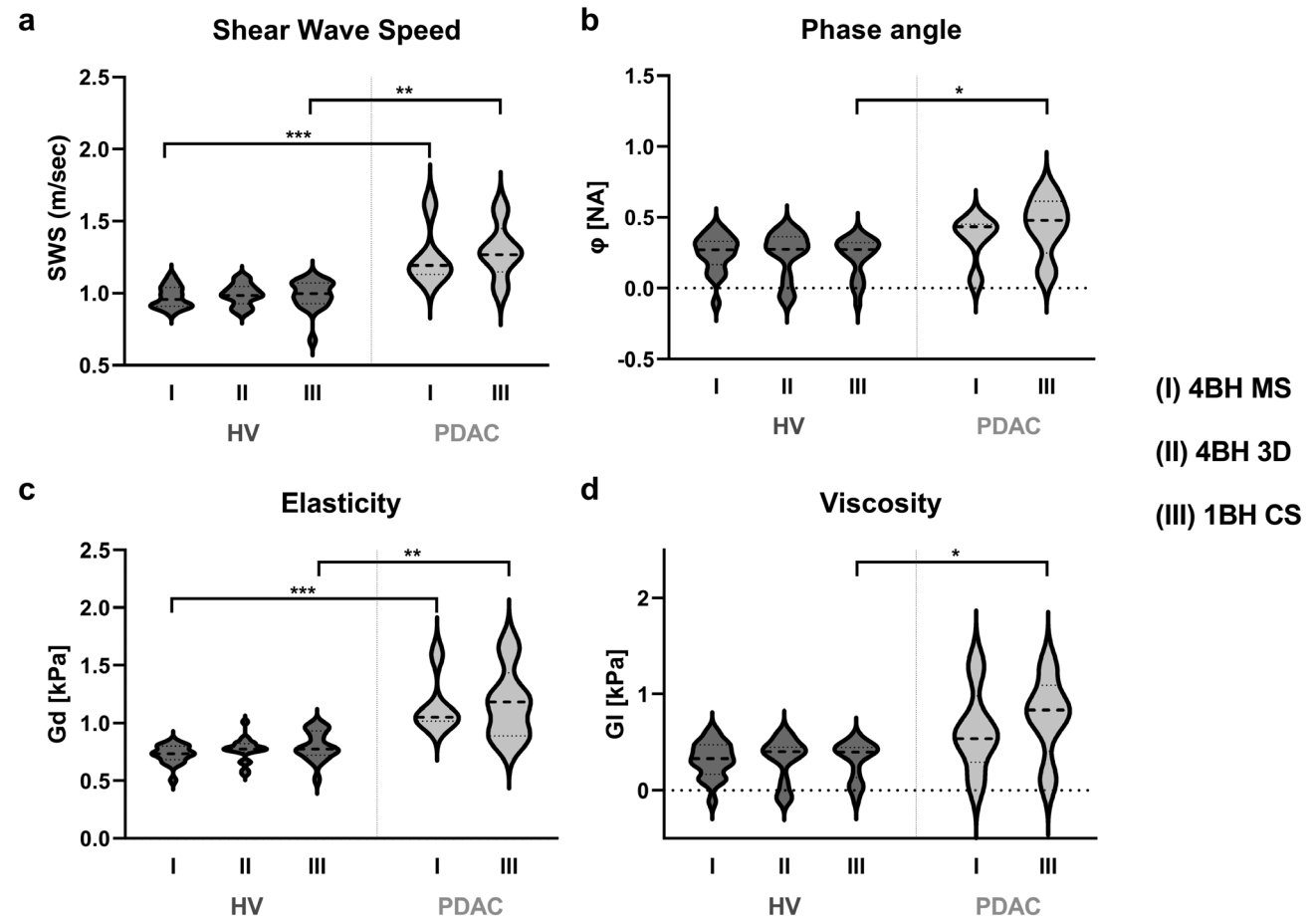


FIGURE 4: Visco-elastic parameters: (a) shear wave speed (SWS), (b) phase angle (ϕ), (c) elasticity (G_d), and (d) viscosity (G_1), for all scans. I) MS 4 breath-hold, II) 3D sense accelerated 4 breath-holds, and III) 3D compressed sensing accelerated single breath-hold for the pancreas head in healthy volunteers and tumor in PDAC patients. Mean values for healthy volunteers and PDAC patients are compared separately for scan I and III (* $P \leq .05$, ** $P \leq .01$, *** $P \leq .001$).

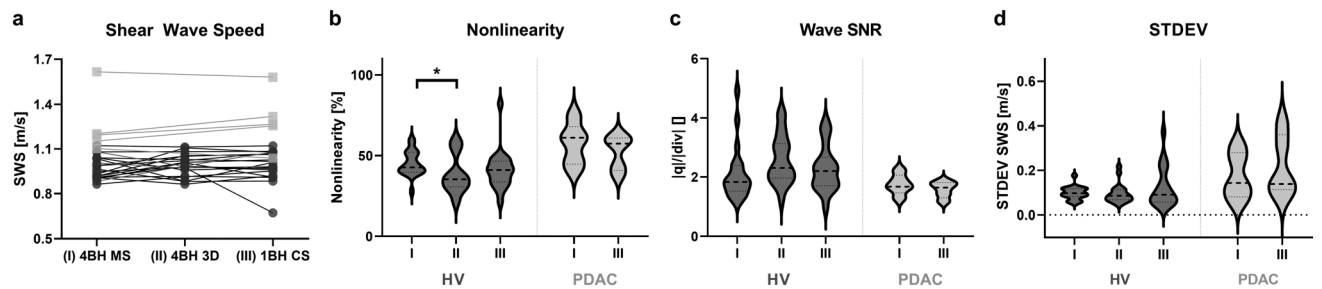


FIGURE 5: (a) Healthy volunteers in blue and PDAC tumor SWS in red; (b) nonlinearity for healthy volunteers (HV) and patients (PDAC); (c) Curl over divergence (wave SNR) for HV and PDAC; (d) STDEV within the ROI for healthy volunteers (HV) and patients (PDAC) (* $P \leq .05$).

nonlinearity, and the capability of clinical implementation with a feasible breath-hold time.

Experiment 2: Implementation of Prospective Undersampling and CS Reconstruction for Single Breath-Hold Ristretto GRE-MRE

In Figs. 2 and 3, shear wave speed and phase angle maps are shown of a representative patient for each scan. Comparison of visco-elastic parameters between scans revealed no differences

in healthy volunteers ($F[2, 38] = 0.462, 0.789, 2.620, 0.054$, and $P = .633, .462, .086, .948$ for SWS, ϕ , G_d , and G_1 , respectively). Similarly, no significant differences were observed in patients between scans I and III ($P = .225, .345, .893, .498$ for SWS, ϕ , G_d , and G_1 , respectively). The findings for both healthy volunteers and PDAC patients are summarized in Table 3 and Fig. 4.

The results showed significant differences in all visco-elastic parameters between healthy volunteers and PDAC

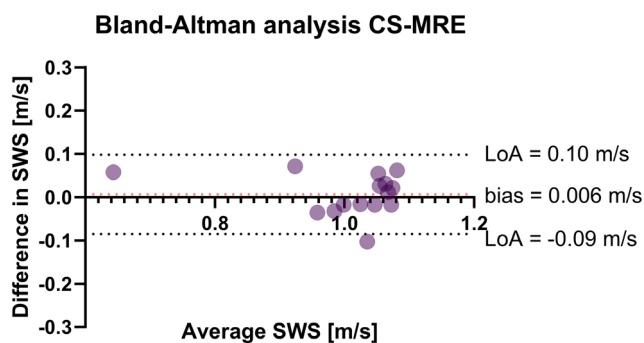


FIGURE 6: Bland–Altman analysis of the repeatability of the shear wave speed (SWS). Limits-of-agreement (LoA) were -0.09 and 0.10 m/second and the bias was -0.006 m/second.

patients (Fig. 4). However, phase angle and viscosity differences were not evident in scan I (φ : $P = .083$ and G_i : $P = .060$). The ratio for SWS of healthy pancreatic tissue in healthy volunteers and tumor tissue in patients with PDAC were 0.71 and 0.72 for scans I and III, respectively.

Figure 5 summarizes comparisons of MRE quality parameters between MS (I) and 3D MRE (II) with 4 breath-holds and the single breath-hold CS MRE (III). A significant decrease was found in nonlinearity in healthy volunteers between scans I and II. Nonetheless, wave SNR and SD within an ROI of the SWS demonstrated no significant differences ($F[2, 38] = 2.312$, $P = .113$ and $F[2, 38] = 1.435$, $P = .251$, respectively).

Experiment 3: Repeatability of Compressed Sensing

The average visco-elastic parameters for scan 1 and scan 2 both were 0.97 ± 0.07 m/second. Bland–Altman analysis of the average SWS showed limits of agreement (LoA) of $[-0.09, 0.10]$ m/second and a bias of -0.006 m/second (Fig. 6). LoA for the φ were $[-0.12, 0.11]$ rad. For SWS the within-subject CoV was 4.8%.

Discussion

Ristretto GRE-MRE accelerated with CS (CS-MRE) allows a single breath-hold MRE acquisition with comparable MRE parameters as conventional four breath-hold multi-slice Ristretto MRE. In addition, both methods displayed comparable MRE quality parameters, such as nonlinearity and wave SNR. Differences were found in pancreatic SWS and elasticity between healthy volunteers and patients with PDAC. These significant differences also hold for the single breath-hold acquisition. We found no significant differences in viscosity nor phase angle in a four breath-hold acquisition between healthy volunteers and patients with PDAC. However, differences were found between healthy volunteers and patients with PDAC for viscosity and phase angle when accelerating to a single breath-hold acquisition.

The increased SWS in PDAC patients could be correlated to the increased stiffness of tumorous tissue. Differences in tumor stiffness have been hypothesized to be related to stromal disposition and have been utilized by surgeons by means of palpation.³¹ Moreover, the phase angle, which is the ratio of elasticity over viscosity, has been associated with the fluidity of soft tissue. Previously published literature that looked at the shear modulus phase angle found a difference between healthy volunteers and PDAC.³² The increase in viscosity and phase angle found when accelerating up to a single breath hold could be caused by high vascularity and permeable vessels, the existence of necrotic tissue, or a shift in the amount of collagen.³³

The ratio of SWS between healthy pancreatic tissue of healthy volunteers and tumor tissue in patients remained similar for the multi breath-hold and a single breath-hold acquisition. These findings may indicate that a single breath-hold acquisition can still differentiate between healthy and diseased pancreatic tissue. Furthermore, the SWS for healthy pancreas and PDAC were overall lower when compared to previously published literature performed at a 40-Hz vibration frequency.^{10,34} This could be due to differences in inversion algorithms. While a direct inversion is most commonly used, the assumptions such as local homogeneity or incompressibility vary. The differences found in stiffness between healthy volunteers and patients with PDAC were comparable to previously published studies for both the four and single breath-hold MRE acquisitions.^{10,32,35}

Imaging with CS has become widely used in a number of clinical applications.³⁶ The choice for an acceleration factor of 12 was determined through careful balancing of scan time (a clinically feasible single breath-hold time for healthy controls and patients of <18 seconds), the loss of spatial resolution introduced by the undersampling, the 3D volumetric coverage (large enough to cover the entire pancreatic head/tumor), and the use of the optimal scan parameters from experiment 1. While sampling and reconstruction parameters were empirically optimized for these criteria, further research is warranted for single breath-hold CS-MRE in other organs, FOVs, or disease types.

The use of a 3D approach in CS-MRE did not have a negative impact on the acquisition efficacy. The flip angle was optimized for the 3D acquisition, which led to an adjusted flip angle of 10 degrees to accommodate the repeated whole-volume excitation compared to 20 degrees in a multi-slice acquisition. Although the longer TR will decrease signal intensity, this is counteracted by a $\sqrt{3}$ gain in signal intensity achievable with the 3D approach. Moreover, a 3D acquisition allows for lower motion encoding gradient frequencies at a fixed TE, due to a shorter radio frequency (RF) pulse and slab selective gradients, thereby increasing encoding efficiency.

Pancreatic MRE using a gravitational transducer and a Ristretto GRE-MRE sequence with fractional motion

encoding is feasible. Wave penetration may be the most important factor in the pancreas and was crucial for successful pancreatic MRE. With decreasing shear wave amplitudes, the shear wave displacement may be lower than the noise level and hence becomes indistinguishable from noise.³⁷ Therefore, a mechanical frequency of 40 Hz was chosen as the optimal frequency for application in the pancreas. Compared with other MRE setups which use multiple transducers,^{11,38} the single gravitational transducer here was situated near the pancreatic tumor. Multiple transducers may provide a greater depth of penetration but come at the cost of destructive wave interference. Furthermore, discretization effects can introduce errors if there are not enough pixels sampled per wavelength. It has been reported that the optimal ratio is six to nine voxels per wavelength for direct inversions.⁷ The ratio in healthy volunteers was 8 voxels per wavelength for both 40 Hz and 50 Hz, indicating that both methods are within the appropriate range. For tumor tissue this ratio increases up to 10, thus indicating that the wavelength becomes larger than the voxel size and inversion could be highly affected by low SNR.

The results obtained for both the within-subject CoV and LoA showed improved results compared to previously published work.^{10,14,39,40} Shi et al reported a lower within-subject CoV of 13.4% at 40 Hz compared to 60 Hz.¹⁰ An et al reported 95% LoA of $[-0.51, 0.60]$ kPa between two scans obtained a day apart.³⁹ These improved results support the hypothesis of superior repeatability that would result from the stable positioning of the pancreas within a single breath-hold compared to deviations in positioning between multiple breath-holds for the other acquisitions. Nonetheless, in a more recent study by Shi et al, the 95% LoA reported were $[-0.072, 0.088]$ m/second at an approximately 7-day interval using a multi-frequency approach.⁴⁰

Limitations

Only a very small cohort of patients with PDAC was included. To investigate differences in underlying mechanical structures within the patient population a larger cohort is necessary. Furthermore, in this study no validation of measured biomechanical properties through histopathology or ex vivo shear testing was done. Ex vivo validation is warranted to substantiate the findings and ensure accuracy. Moreover, the gravitational transducer allows for high amplitude shear waves with accuracy in inversion due to the precise fundamental vibration frequency. However, this single transducer approach does not easily allow adjustable placement and due to the high intrinsic attenuation of shear waves, caused by gas or scattering in the abdomen, vibration of the entire abdomen is challenging from a single point of shear wave introduction (i.e., a single transducer). Lastly, the nonlinearity was slightly higher in PDAC patients compared to healthy volunteers for

the multi and single breath-hold acquisitions, stretching towards 50%. However, accuracy of MRE inversion is only guaranteed for a nonlinearity below 50%, thus our findings could be considered borderline acceptable as the ROI shows an average nonlinearity that is just below 50%.¹⁶ Moreover, for some individual pixels viscosity values were found below zero, which is in violation of conservation of energy and gives an indication for insufficient data quality for assessment of this parameter. This could be caused by the low mechanical frequency and the high acceleration factor that could hamper precision in the inversion, especially in tissues with high stiffness. However, this increase was not substantial compared to nonlinearity and viscosity in healthy volunteers, indicating that this effect is negligible for acceleration up to a single breath-hold. Further research is necessary to ascertain differences within PDAC patients in quantification of stromal disposition and investigate the possibility of single breath-hold MRE as a biomarker for PDAC chemotherapy efficacy.

Conclusion

The use of Ristretto GRE-MRE accelerated with CS may allow for a single breath-hold MRE acquisition with comparable SWS as four breath-hold multi-slice Ristretto MRE. The differences found in SWS and phase angle between healthy volunteers and patients with PDAC were comparable for both the four and single breath-hold MRE.

References

1. Orth M, Metzger P, Gerum S, et al. Pancreatic ductal adenocarcinoma: biological hallmarks, current status, and future perspectives of combined modality treatment approaches. *Radiat Oncol* 2019;14(1):141.
2. Walma MS, Brada LJ, Patuleia SIS, et al. Treatment strategies and clinical outcomes in consecutive patients with locally advanced pancreatic cancer: A multicenter prospective cohort. *Eur J Surg Oncol* 2021;47:699-707.
3. Perri G, Prakash L, Qiao W, et al. Response and survival associated with first-line FOLFIRINOX vs gemcitabine and nab-paclitaxel chemotherapy for localized pancreatic ductal adenocarcinoma. *JAMA Surg* 2020;155(9):832-839.
4. Wang D, Li Y, Ge H, Ghadban T, Reeh M. The extracellular matrix: A key accomplice of cancer stem cell migration, metastasis formation, and drug resistance in PDAC. *Cancer* 2022;14:3998.
5. Erkan M, Hausmann S, Michalski CW, et al. How fibrosis influences imaging and surgical decisions in pancreatic cancer. *Front Physiol* 2012;3:389.
6. Nissan N. Modifications of pancreatic diffusion MRI by tissue characteristics: what are we weighting for? *NMR Biomed* 2017;30(8):e3728.
7. Manduca A, Bayly PJ, Ehman RL, et al. MR elastography: Principles, guidelines, and terminology. *Magn Reson Med* 2020;85:2377-2390.
8. Guo J, Savic L, Hillebrandt K, Sack I. MR elastography in cancer. *Investig Radiol* 2023;00(00):1-9.
9. Zhuo J, Gullapalli RP. MR artifacts, safety, and quality control. *RadioGraphics* 2006;26(1):275-297.
10. Shi Y, Glaser KJ, Venkatesh SK, Ben-Abraham EI, Ehman RL. Feasibility of using 3D MR elastography to determine pancreatic stiffness in healthy volunteers. *J Magn Reson Imaging* 2015;41:369-375.

11. Dittmann F, Tzschätzsch H, Hirsch S, et al. Tomoelastography of the abdomen: Tissue mechanical properties of the liver, spleen, kidney, and pancreas from single MR elastography scans at different hydration states. *Magn Reson Med* 2017;78:976-983.
12. Tirkes T, Yadav D, Conwell DL, et al. Magnetic resonance imaging as a non-invasive method for the assessment of pancreatic fibrosis (MINIMAP): A comprehensive study design from the consortium for the study of chronic pancreatitis, diabetes, and pancreatic cancer. *Abdom Radiol* 2019;44:2809-2821.
13. Steinkohl E, Olesen SS, Hansen TM, Drewes AM, Frøkjær JB. T1 relaxation times and MR elastography-derived stiffness: New potential imaging biomarkers for the assessment of chronic pancreatitis. *Abdom Radiol* 2021;46:5598-5608.
14. Kolipaka A, Schroeder S, Mo X, Shah Z, Hart PA, Conwell DL. Magnetic resonance elastography of the pancreas: Measurement reproducibility and relationship with age. *Magn Reson Imaging* 2017;42:1-7.
15. Guenther C, Sethi S, Troelstra M, Dokumaci AS, Sinkus R, Kozerke S. Ristretto MRE: A generalized multi-shot GRE-MRE sequence. *NMR Biomed* 2019;32:e4049.
16. Runge JH, Hoelzl SH, Sudakova J, et al. A novel magnetic resonance elastography transducer concept based on a rotational eccentric mass: Preliminary experiences with the gravitational transducer. *Phys Med Biol* 2019;64:045007.
17. Troelstra MA, Witjes JJ, van Dijk AM, et al. Assessment of imaging modalities against liver biopsy in nonalcoholic fatty liver disease: The Amsterdam NAFLD-NASH cohort. *J Magn Reson Imaging* 2021;54(6):1937-1949.
18. Sinkus R, Lambert S, Abd-Elmoniem KZ, et al. Rheological determinants for simultaneous staging of hepatic fibrosis and inflammation in patients with chronic liver disease. *NMR Biomed* 2018;31(10):e3956.
19. Lustig M, Donoho D, Pauly JM. Sparse MRI: The application of compressed sensing for rapid MR imaging. *Magn Reson Med* 2007;58(6):1182-1195.
20. Blanken CPS, Schrauben EM, Peper ES, et al. Coronary flow assessment using accelerated 4D flow MRI with respiratory motion correction. *Front Bioeng Biotechnol* 2021;9:725833.
21. de Jonge CS, Coolen BF, Peper ES, et al. Evaluation of compressed sensing MRI for accelerated bowel motility imaging. *Eur Radiol Exp* 2019;3:7.
22. Gottwald LM, Peper ES, Zhang Q, et al. Pseudo-spiral sampling and compressed sensing reconstruction provides flexibility of temporal resolution in accelerated aortic 4D flow MRI: A comparison with k-t principal component analysis. *NMR Biomed* 2020;33(4):e4255.
23. Steinkohl E, Bertoli D, Hansen TM, Olesen SS, Drewes AM, Frøkjær JB. Practical and clinical applications of pancreatic magnetic resonance elastography: a systematic review. *Abdom Radiol* 2021;46(10):4744-4764.
24. Parkes M, Cashmore J, Green S, et al. Defining short and prolonged breath-holds. *Br J Radiol* 2020;93:2020019.
25. Ye JC. Compressed sensing MRI: A review from signal processing perspective. *BMC Biomed Eng* 2019;1:8.
26. Uecker M. *Berkeley Advanced Reconstruction Toolbox*. Toronto, Canada: International Society of Magnetic Resonance in Medicine; 2015.
27. Beck A, Teboulle M. A fast iterative shrinkage-thresholding algorithm for linear inverse problems. *SIAM J Imaging Sci* 2009;2(1):183-202.
28. Fovargue D, Kozerke S, Sinkus R, Nordsletten D. Robust MR elastography stiffness quantification using a localized divergence free finite element reconstruction. *Med Image Anal* 2018;44:126-142.
29. Prezzi D, Neji R, Kelly-Morland C, et al. Characterization of small renal tumors with magnetic resonance elastography. *Investig Radiol* 2018;53(6):344-351.
30. Bland JM. Statistical methods for assessing agreement between two methods of clinical measurement. *Lancet* 1986;327:307-310.
31. Narkhede RA, Desai GS, Prasad PP, Wagle PK. Diagnosis and management of pancreatic adenocarcinoma in the background of chronic pancreatitis: Core issues. *Dig Dis* 2019;37(4):315-324.
32. Zhu L, Guo J, Jin Z, et al. Distinguishing pancreatic cancer and autoimmune pancreatitis with in vivo tomoelastography. *Eur Radiol* 2021;31:3366-3374.
33. Shahyari M, Meyer T, Warmuth C, et al. Reduction of breathing artifacts in multifrequency magnetic resonance elastography of the abdomen. *Magn Reson Med* 2021;85:1962-1973.
34. Shi Y, Cang L, Zhang X, et al. The use of magnetic resonance elastography in differentiating autoimmune pancreatitis from pancreatic ductal adenocarcinoma: A preliminary study. *Eur J Radiol* 2018;108:13-20.
35. Itoh Y, Takehara Y, Kawase T, et al. Feasibility of magnetic resonance elastography for the pancreas at 3T. *J Magn Reson Imaging* 2016;43:384-390.
36. Smith DS, Li X, Abramson RG, Quarles CC, Yankeelov TE, Welch EB. Potential of compressed sensing in quantitative MR imaging of cancer. *Cancer Imaging* 2013;13(4):633-644.
37. Papazoglou S, Xu C, Hamhaber U, et al. Scatter-based magnetic resonance elastography. *Phys Med Biol* 2009;54:2229-2241.
38. Gültekin E, Wetz C, Braun J, et al. Added value of tomoelastography for characterization of pancreatic neuroendocrine tumor aggressiveness based on stiffness. *Cancer* 2021;13:5185.
39. An H, Shi Y, Guo Q, Liu Y. Test-retest reliability of 3D EPI MR elastography of the pancreas. *Clin Radiol* 2016;71:1068.e1067-e1012.
40. Shi S, Wang L, Peng Z, et al. Multi-frequency magnetic resonance elastography of the pancreas: Measurement reproducibility and variance among healthy volunteers. *Gastroenterol Rep* 2022;10:1-7.